Analysis of Dynamic Current Control Techniques for Switched Reluctance Motor Drives for High Performance Applications

Siddharth Mehta
FREEDM Systems Center, Dept. of ECE
North Carolina State University
Raleigh, USA
smehta5@ncsu.edu

Prerit Pramod
Research & Development
Nexteer Automotive Corporation
Saginaw, USA
prerit.pramod@nexteer.com

Iqbal Husain
FREEDM Systems Center, Dept. of ECE
North Carolina State University
Raleigh, USA
ihusain2@ncsu.edu

Abstract—**Current controllers form a crucial part of a switched reluctance motor (SRM) drive control system because they significantly impact the overall drive performance from multiple standpoints including steady-state capability, dynamic response as well as noise and vibration performance. This paper presents a comparative analysis of two current control methods for SRM drive systems namely conventional proportional-integral control and predictive deadbeat control. The controllers are assessed and compared for different performance metrics including command tracking behavior, disturbance rejection capability, noise transmission characteristics as well as robustness to modeling uncertainty (parameter estimation errors). The presented analysis greatly simplifies the selection process for determining the best current control technique for a given application with specific performance requirements. The current controller design and analysis is performed through simulations on a practical 12 V, fractional kW 12-slot, 8-pole SRM.**

Index Terms—**switched reluctance machine, electric motor drive, current control, dynamics, torque ripple minimization, predictive control, deadbeat control, bandwidth, disturbance rejection, sensor noise transmission, digital control, discrete-time analysis**

I. Introduction

Switched reluctance motor (SRM) drives are strong contenders for several industrial applications due to their rugged and simple construction, relatively low and involatile cost particularly due to the absence of permanent magnets, zero cogging torque and fault tolerant operation capability and thus reliability. SRMs however suffer from the disadvantage of poor noise, vibration and harness (NVH) performance due to both torque ripple and structural vibration, and therefore, considered unfit for high control performance applications such as electric power steering (EPS). Extensive research has been conducted on development of both machine design based passive and control based active techniques for improvement of the NVH performance [1]–[4]. For the majority of the active control based approaches, the general methodology is to utilize a model of the torque ripple and/or radial force variation to develop current command profiles that, if generated accurately, can eliminate the undesirable torque ripple and structural vibration. It has been shown that the torque ripple can be brought to a level less than 5% [2] but the results are applicable for only a specific, limited set of operating conditions. To achieve that level of performance in the majority of the operating region, it is essential to understand the behavior of the motor current controller, particularly the factors that affect its desired performance. The current controller plays a significant role in influencing the overall drive performance from a steady-state capability, dynamic performance and NVH performance standpoint, and is therefore a critical part of the overall SRM drive system. Thus, the accuracy and bandwidth with which the current tracking is achieved is a direct function of the characteristics of the current controller. These properties of the controller are impacted by various factors including the control parameters such as gains, modeling uncertainty, i.e., errors in estimation of machine parameters, disturbance inputs such as the back-EMF (BEMF) of the machine and sensor noise, among others. While some literature does exist on different current control techniques and their relative performance comparison [5]–[9], a systematic analysis of the state-of-the-art current controllers has not been performed previously. The performance of a predictive controller and a conventional proportional-integral (PI) controller is analyzed and illustrated in this paper. A comparison of these two controllers using a structured approach is presented in order to allow for easy selection of the optimal control technique for a given application with specific performance requirements. The theoretical description is validated by extensive simulation results on a prototype 12 V, fractional kW, 12-slot 8-pole (12/8) SRM.

II. Linear Modeling of SRM Drive System

The governing equations for SRMs that constitute the plant model are given in (1)-(3).

$$V_x = L_{inc(x)}\dot{I}_x + R_x I_x - \omega_e \lambda_{inc(x)} \quad (1)$$

$$\lambda_{inc(x)} = \frac{\partial \lambda_x}{\partial \theta} \quad (2)$$

$$L_{inc(x)} = \frac{\partial \lambda_x}{\partial I_x} \qquad (3)$$

where x represents the phase under consideration, V is the termnial voltage input, I is the phase current, L_{inc} is the incremental inductance, λ_{inc} is the incremental flux linkage, R is the circuit resistance including the motor windings and the power converter switches, θ is the rotor electrical position and ω_e is the rotational electrical velocity. In reality, both $L_{inc(x)}$ and $\lambda_{inc(x)}$ vary with current due to magentic saturation and with position due to the existence of harmonics. However, for linear analysis, both these effects are ignored and the two quantities are assumed to be constant. Further, the resistance of the machine circuit R_x is affected by the temperature of the windings as well as the switches used in the power converter. The back-EMF voltage E may be expressed as (4).

$$E = \omega_e \lambda_{inc} \qquad (4)$$

Although the electromagnetic torque T_e is not required for the analysis of the current controller, it is provided here for the sake of completeness. The torque for a single phase is expressed in (5).

$$T_x = \frac{1}{2} \frac{\partial L_{(x)}}{\partial \theta} i_x^2 \qquad (5)$$

The current control system, in addition to the motor itself, consists of the power converter, the current controller and the current measurement circuit as shown in Fig. 1.
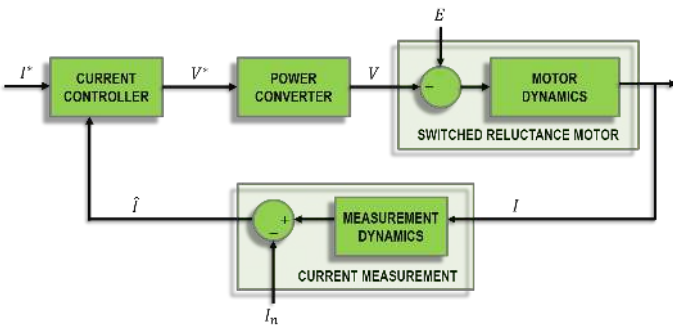

Fig. 1. Block diagram of the SRM drive current control system.

The phase current is sensed using a current measurement circuit which exhibits a transport delay and is usually corrupted by random sensor noise I_n. The measured current $\hat{I}$ is then used along with the commanded current I^* by the current controller to generate a desired duty cycle or voltage command V^*. In most embedded real-time motor drive applications, the current controller is implemented as an interrupt service routine (ISR), which is triggered by the successful completion of the current measurement. The application of the voltage is performed using Pulse Width Modulation (PWM), which causes a delay equal to the switching or PWM time period T. The current controller is assumed to be a general two-degree-of-freedom (2DOF) control architecture which scales

the current command I^* by one compensation term and the measured current $\hat{I}$ by a separate compensator. In addition, a disturbance feedforward term D is also included (not shown) which, in the case of SRMs, is for BEMF compensation.

The parameters of the 12S-8P SRM used in the analysis presented in this paper are shown in Table I.

TABLE I
MOTOR PARAMETERS

Parameter	Value
Rated Power (W)	250
Rated Torque (Nm)	2.4
Base Speed (RPM)	1000
DC Link Voltage (V)	12
Winding Resistance ($m\Omega$)	65
Sampling Time (µs)	50
Rated Un-anligned Inductance (µH)	45
Switching Frequency (kHz)	20

III. CURRENT CONTROL TECHNIQUES

As mentioned earlier, the current control system forms a critical part of the SRM drive system. Beyond providing accurate tracking bandwidth, the system is required to perform accurate current command under variable frequency inputs, provide adequate disturbance rejection, have high sensor noise immunity and be robust to modeling uncertainty. The current commands are typically profiled, i.e., scheduled as a function of position and current, in order to eliminate torque ripple and radial force variation. With varying velocity during operation, the rate of change of the current commands can change significantly, resulting in inaccurate current tracking, ultimately resulting in poor NVH characteristics. Further, the fact that the parameters of the machine vary non-linearly with operating condition due to magnetic saturation, presence of harmonics and due to temperature variation, the robustness of the current control system is extremely important.

The two most commonly employed current control techniques, namely proportional-integral (PI) control and predictive deadbeat (DB) control, are analyzed in this section. Specifically, the performance metrics of command tracking response, disturbance rejection and noise transmission are evaluated and compared. Further, the robustness of the controllers to modeling uncertainty is also studied.

A. Proportional Integral Control

PI controllers utilize integral control to provide steady state tracking to step command inputs while the proportional component allows for faster dynamic response. These controllers allow active bandwidth tuning through the tuning of the controller parameters K_p and K_i which is helpful for achieving balanced control performance in terms of command tracking, disturbance rejection and noise transmission. The commanded voltage from the PI controller in discrete time can be written as (6).

$$V^*_{PI}(z) = C_{PI}(z)(I^*(z) - \hat{I}(z)) + \hat{E}(z);$$
$$= \Big(K_p + \frac{K_i T}{1 - z^{-1}}\Big)(I^*(z) - \hat{I}(z)) + \hat{E}(z) \qquad (6)$$

where $\hat{E}$ is the estimated BEMF term and the integrator is discretized using the backward difference method.

The PI controller is tuned by using the zero to cancel the plant pole and the additional parameter ω_b that is introduced as a result represents the desired bandwidth of the closed-loop system. The PI controller may then be expressed as (7).

$$C_{PI}(z) = \omega_b\Big(\hat{L}_{inc} + \frac{\hat{R}T}{1 - z^{-1}}\Big) \qquad (7)$$

In order to perform the control current system analysis in the continuous frequency domain, the transfer function of PI controller is computed by replacing z^{-1} by e^{-Ts} which results in (8).

$$C_{PI}(s) = \omega_b\Big(\hat{L}_{inc} + \frac{\hat{R}T}{\hat{s}}\Big)$$
$$\hat{s} = \frac{1 - e^{-Ts}}{T} \qquad (8)$$

Three transfer functions namely the command tracking transfer function G_{iPI}, the disturbance rejection transfer function G_{dPI} and noise transmission transfer function G_{nPI} are considered for comparing the performance of the two current control designs. The output of the PI controller in terms of the command may be written in terms of these transfer functions as (9).

$$I(s) = G_{iPI}(s)I^*(s) + G_{dPI}E(s) + G_{nPI}I_n(s) \qquad (9)$$

The command tracking and noise transmission functions are identical, as is always the case with 1-degree-of-freedom (1-DOF) control architectures and are expressed as (10).

$$G_{iPI} = G_{nPI} = \frac{e^{-Ts}\omega_b(\hat{L_{inc}}\hat{s} + \hat{R})}{(L_{inc}s + R)\hat{s} + e^{-Ts}\omega_b(\hat{L_{inc}}\hat{s} + \hat{R})} \qquad (10)$$

The disturbance rejection transfer function, with r being a scaling term representing estimation error in BEMF, is obtained as (11).

$$G_{dPI} = \frac{\hat{s}(e^{-Ts}r - 1)}{(L_{inc}s + R)\hat{s} + e^{-Ts}\omega_b(\hat{L_{inc}}\hat{s} + \hat{R})} \qquad (11)$$

The analysis of the PI controller is performed through a study of the impact of the primary control parameters, namely the desired closed-loop bandwidth, sampling or PWM period and modeling uncertainty.

1) Performance Analysis: Frequency response plots illustrating the effects of the bandwidth tuning parameter on the command tracking, disturbance rejection and noise transmission characteristics are shown in Fig. 2. Increase in desired bandwidth results in higher cutoff frequency response characteristics, i.e., in terms of the gain attenuation and phase delay. Fig. 2(a) illustrates that as bandwidth increases from 200 Hz up to 3000 Hz, the -3 dB gain occurs at 191 Hz and 6636 Hz, while the -45^0 phase delay point changes from 191 Hz to 2156 Hz. This implies that the magnitude response shape deviates significantly from that of a first order system while the phase delay is higher than expected. Note that this conclusion comes from the fact that the pole zero cancellation would result in an ideal first order response if the time delay effect was negligible. However, as the desired bandwidth increases and becomes comparable to the sampling frequency, the response deviates from the ideal due to the significant impact of the time delay. The noise transmission characteristics shown in Fig. 2(c) change identically as the command tracking response and thus allow higher noise frequency content to pass through as the bandwidth increases. The disturbance rejection characteristics shown in Fig. 2(b) show that the overall magnitude drops in the low frequency range as bandwidth increases and the peak, which occurs at higher frequencies, becomes higher. In the context of SRM drives, this indicates improvement in disturbance rejection, since the primary disturbance is the BEMF estimation error, which is a relatively slowly varying (i.e., low frequency) signal, since it is a state variable of the mechanical system.

2) Sampling Time: Sampling period, which is the rate of execution of the motor current control loop, impacts the overall system response significantly. Apart from switching noise characteristics, time-delays result in more and more oscillatory responses as the desired bandwidth is increased. Fig. 3 illustrates the current control step responses different sampling periods. The plot exemplifies increasingly oscillatory, i.e., less stable, closed-loop tracking behavior as the sampling time period and therefore the time delay increases.

3) Robustness: While PI controllers do suffer from dynamic response degradation due to parameter estimation errors, their steady state step response is consistent due to the presence of the integrator. This is evident from the step responses in Fig. 4 which shows that while the dynamic response is different with inductance estimation errors, the steady state output is unchanged. Resistance errors, as shown in Fig. 5, cause reduction in the low-frequency gain response, but have relatively insignificant impact on the phase responses.

B. Predictive Deadbeat Control

The objective of predictive deadbeat control is to force the system to reach steady state within the minimum possible number of sampling periods. It is a discrete time control technique which utilizes a model of the plant in order to compute the appropriate voltage command. The expression for the voltage command for a predictive deadbeat controller
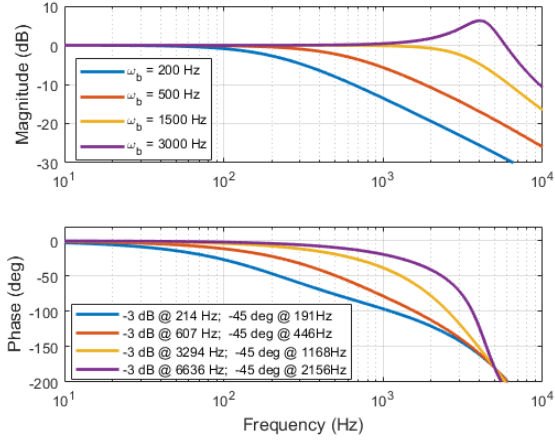
(a)
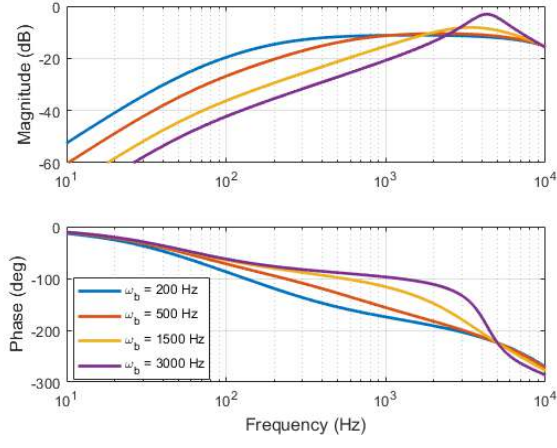
(b)
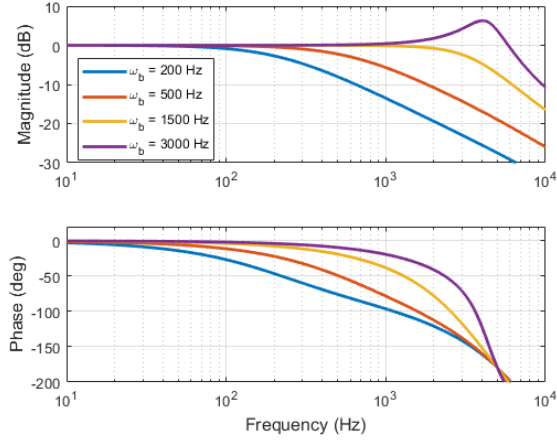
(c)

Fig. 2. PI closed-loop current control (a) command tracking, (b) disturbance rejection (c) noise transmission frequency response characteristics with different bandwidth settings.
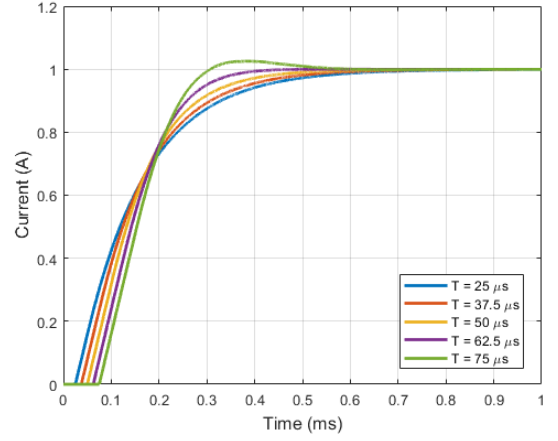

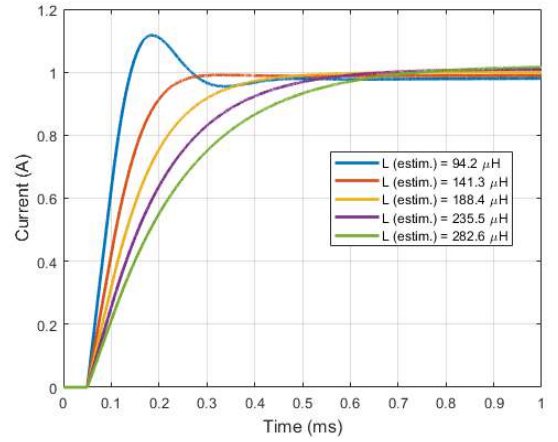Fig. 3. Command tracking step response for PI control with varying sampling time periods.

Fig. 4. Command tracking step responses for PI control with inductance estimation errors.
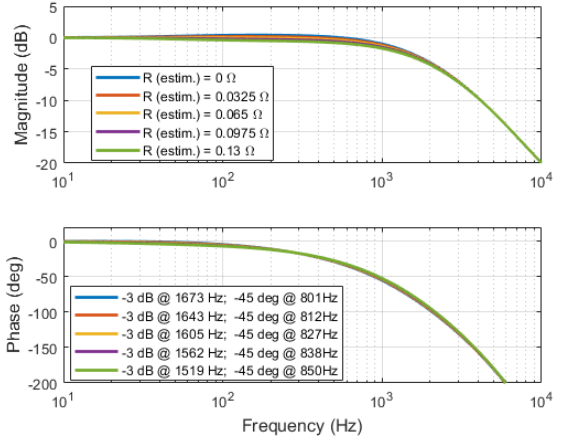

Fig. 5. Command tracking step responses for PI control with inductance estimation errors.

developed using a backward difference approximation of the plant model is given in (12).

$$V_{DB}^*(z) = -z^{-1}V_{DB}^* + \left(\hat{R} + \frac{\hat{L_{inc}}}{T}\right)I^*(z)$$
$$+ \left(\hat{R} - z^{-1}\frac{\hat{L_{inc}}}{T}\right)I(z) + \hat{E}(z)$$

(12)

The closed loop actual current output may be written in terms of the command, disturbance and sensor noise inputs in the continuous time domain as (13). The command tracking transfer function for the predictive deadbeat controller is given in (14).

$$I(s) = G_{iDB}I^*(s) + G_{dDB}E(s) + G_{nDB}I_n(s) \qquad (13)$$

$$G_{iDB} = \frac{(\hat{R}T + \hat{L_{inc}})e^{-Ts}}{(RT + L_{inc}) + (R - \hat{R})Te^{-Ts} + (\hat{L_{inc}} - L_{inc})e^{-2Ts}} \qquad (14)$$

Notice that if the parameter estimates are assumed to be accurate, the closed loop command tracking transfer function becomes a pure delay of one sampling time period. The disturbance rejection and noise transmission transfer functions are expressed as (15) and (16) respectively. The detailed analysis of predictive deadbeat current control performance is presented next.

$$G_{dDB} = \frac{(T((r+1)e^{-Ts} - 1)}{(RT + L_{inc}) + (R - \hat{R})Te^{-Ts} + (\hat{L_{inc}} - L_{inc})e^{-2Ts}} \qquad (15)$$

$$G_{nDB} = \frac{(-\hat{R}T + \hat{L_{inc}})e^{-Ts}}{(RT + L_{inc}) + (R - \hat{R})Te^{-Ts} + (\hat{L_{inc}} - L_{inc})e^{-2Ts}} \qquad (16)$$

1) Performance Analysis: The closed-loop current command tracking, disturbance rejection and noise transmission characteristics of the SRM drive system with predictive deadbeat control is shown in Fig. 6.

Since the responses plotted are obtained under ideal parameter estimation conditions, the command tracking behavior is that of a pure time delay which is exemplified by the constant 0 dB gain characteristic across all frequencies and phase delay similar to that of a pure transport lag. The disturbance rejection transfer function shows relatively constant gain at lower frequencies and increases as the input frequency increases. Since the disturbance input is the BEMF voltage which has low frequency content, the disturbance rejection characteristics are consistent. The noise transmission characteristic is virtually equivalent to the command tracking response, i.e., high bandwidth which implies that the deadbeat controller allows the entire noise spectra to pass through and corrupt the output current signal.

2) Sampling Time: The command tracking responses of the predictive deadbeat controller with different sampling frequencies, shown in Fig. 7, illustrates the expected ideal one sample time step delay tracking.

3) Robustness: The robustness of the predictive deadbeat controller to modeling uncertainty is presented in this section. The step responses for current command tracking with different inductance estimation errors are illustrated in Fig. 8. These response exemplify that overestimation of inductance results in an oscillatory, less stable response while underestimation causes the response to become sluggish.
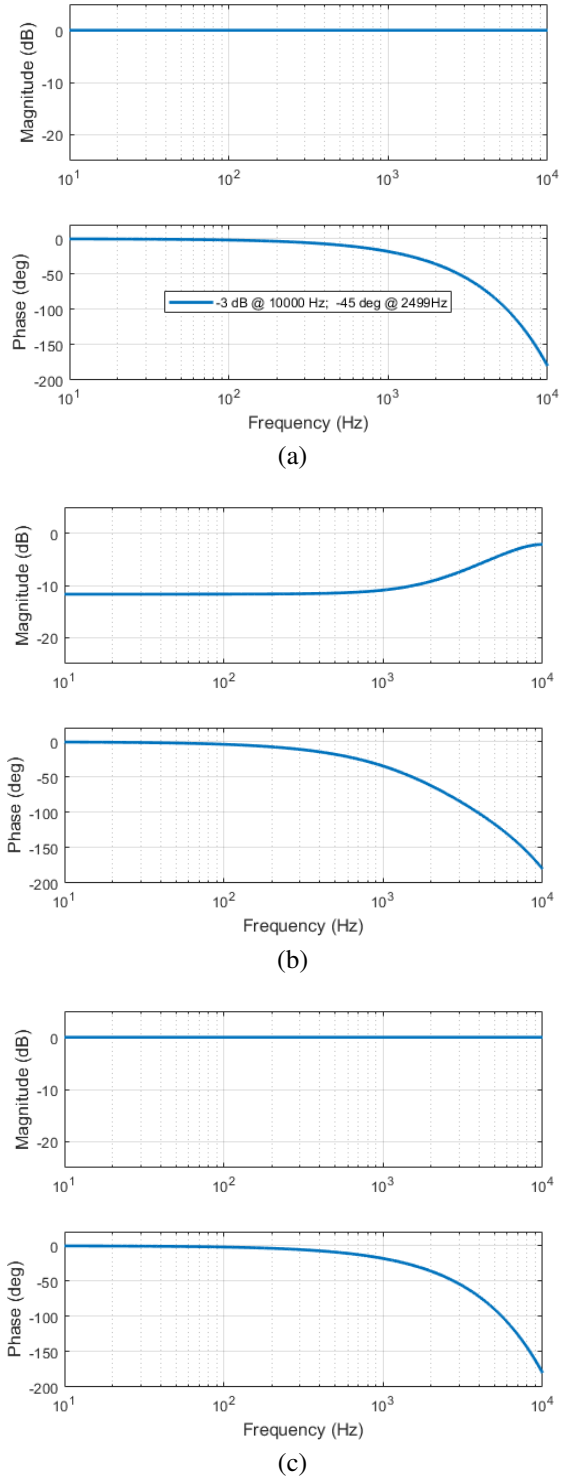

Fig. 6. Predictive deadbeat closed-loop current control (a) command tracking, (b) disturbance rejection (c) noise transmission frequency response characteristics.

The effect of resistance estimation errors on the performance is shown in Fig. 9. As indicated by the frequency responses, resistance errors result in a non-zero DC gain which implies a steady state tracking error. However, the phase response is
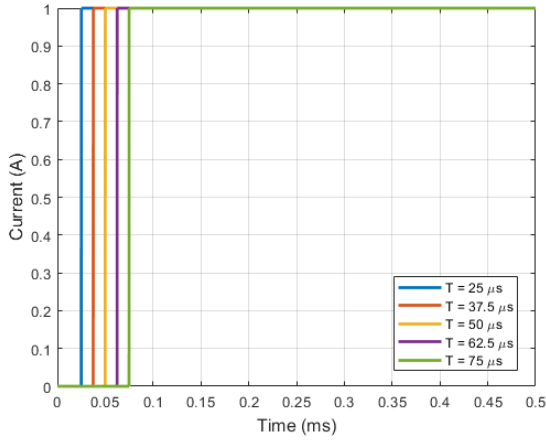
Fig. 7. Command tracking step responses for predictive deadbeat control with inductance estimation errors.
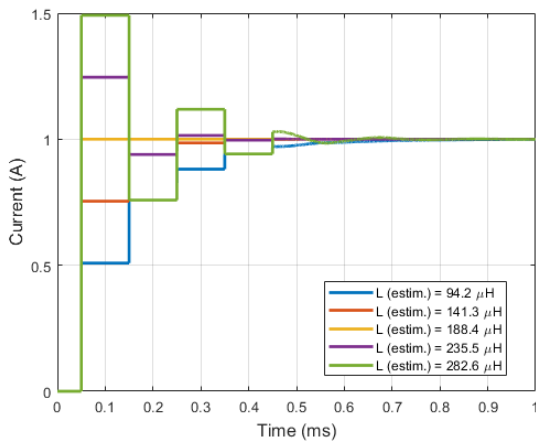

Fig. 8. Command tracking step responses for predictive deadbeat control with inductance estimation errors.
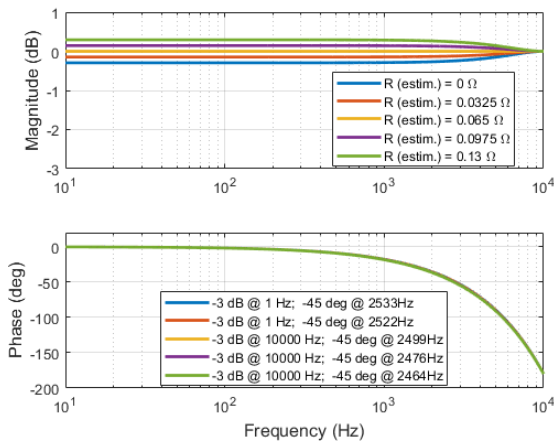

Fig. 9. Command tracking frequency responses for predictive deadbeat control with resistance estimation errors.

virtually unaffected implying that the settling time is relatively consistent even under resistance modeling uncertainty.

IV. PERFORMANCE COMPARISON OF CURRENT CONTROLLERS

The performance of the two current control techniques is presented in this section. A comparison based on the linear analysis performed thus far is presented first, which is followed by non-linear analysis considering practical aspects of SRM drive current control.

A. Linear Performance Comparison

Comparing the command tracking frequency responses for the PI controller with those of the predictive deadbeat controller presented previously, it is clear that the deadbeat controller provides a significantly higher bandwidth, i.e., command magnitude tracking for a higher range of input frequencies as compared to the PI controller. However, the predictive controller, since it is a model-based technique and thus feedforward or open-loop in nature, is much more sensitive to parameter estimation errors as explained in the sensitivity analysis presented earlier.

In terms of disturbance rejection, the predictive controller outperforms the PI controller in terms of the bandwidth under the absence of modeling uncertainty. However, it is not robust when BEMF estimation errors exist. Noise transmission characteristics of the PI controllers are, in general, better than that of the predictive controller, which intuitively follows from the fact that it has lower bandwidth (which is, of course, dependent on the tuning).

B. Non-linear Performance Comparison

As mentioned earlier, SRMs are highly non-linear due to the presence of harmonics in the magnetic flux linkage and torque which is further complicated by the effects of magnetic saturation. Due to these harmonics, the current command is profiled in practical applications in order to minimize harmonics. The profiled currents have a highly non-linear shape with respect to position and thus the current regulator is subjected to a highly variable frequency input when the motor speed changes [3].

Simulation results illustrating the current outputs for the two controllers for a practical SRM drive for a profiled current command at a speed of 100 RPM with nominal current command 40 A is shown in Fig. 10. Note that the simulation includes all the non-linearities of the SRM, but the controllers are linear as described in the previous section. This is done simply for fair comparison of the performance, but it should be noted that in practical applications the implementation is more sophisticated in that the parameters are estimated considering all the non-linear effects.

The responses indicate that the PI controller outperforms the predictive deadbeat controller in this case, which can be attributed to the fact that the latter is very sensitive to modeling errors. However, a more detailed comparison including multiple operating conditions, exogenous inputs and estimation errors is required to understand true performance difference in a practical implementation that incorporates and thus compensates for several of the non-linearities of the SRM.
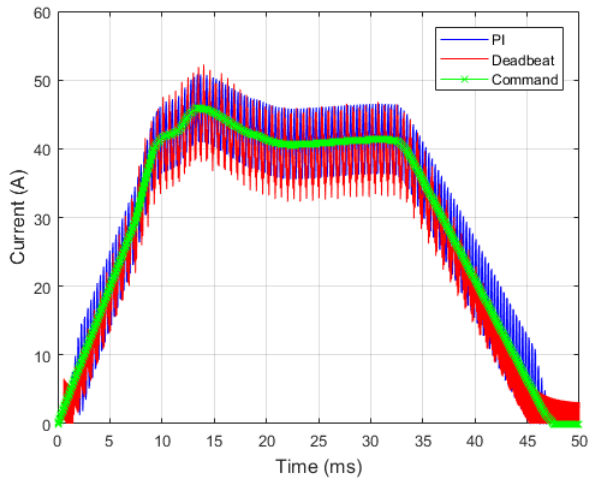
Fig. 10. Comparison of PI and predictive deadbeat current control tracking performance for profiled (position dependent) current command input.

V. CONCLUSION

A systematic comparison of two current control techniques for SRM drives is presented. Frequency domain analysis is utilized to compare the two controllers in terms of their current command tracking, disturbance rejection and noise transmission characteristics. The robustness of the system with both techniques is also presented in order to capture the effects of modeling uncertainty or parameter estimation errors. Finally, the control performance considering a variable frequency current command input obtained from current profiling is also described. The analysis allows for easily selecting the optimal current controller design for an application at hand given its specific performance requirements and constraints.

REFERENCES

[1] J. Ye, P. Malysz, and A. Emadi, "A Fixed-Switching-Frequency integral sliding mode current controller for switched reluctance motor drives," *IEEE Journal of Emerging and Selected Topics in Power Electronics*, vol. 3, no. 2, pp. 381–394, Jun. 2015.

[2] R. Mikail, I. Husain, Y. Sozer, M. S. Islam, and T. Sebastian, "Torque-Ripple minimization of switched reluctance machines through current profiling," *IEEE Trans. Ind. Appl.*, vol. 49, no. 3, pp. 1258–1267, May 2013.

[3] S. Mehta, M. A. Kabir, and I. Husain, "Extended speed current profiling algorithm for low torque ripple SRM using model predictive control," in *2018 IEEE Energy Conversion Congress and Exposition (ECCE)*, Sep. 2018, pp. 4558–4563.

[4] C. Ma, R. Mitra, P. Pramod, and R. Islam, "Investigation of torque ripple in switched reluctance machines with errors in current and position sensing," in *2017 IEEE Energy Conversion Congress and Exposition (ECCE)*, Oct. 2017, pp. 745–751.

[5] F. Blaabjerg, P. C. Kjaer, P. O. Rasmussen, and C. Cossar, "Improved digital current control methods in switched reluctance motor drives," *IEEE Trans. Power Electron.*, vol. 14, no. 3, pp. 563–572, May 1999.

[6] X. Wang and J.-S. Lai, "Small-signal modeling and control for PWM control of switched reluctance motor drives," in *2002 IEEE 33rd Annual IEEE Power Electronics Specialists Conference. Proceedings (Cat. No.02CH37289)*, vol. 2, Jun. 2002, pp. 546–551 vol.2.

[7] R. Mikail, I. Husain, Y. Sozer, M. Islam, and T. Sebastian, "A fixed switching frequency predictive current control method for switched reluctance machines," in *2012 IEEE Energy Conversion Congress and Exposition (ECCE)*, Sep. 2012, pp. 843–847.

[8] S. S. Ahmad and G. Narayanan, "Linearized modeling of switched reluctance motor for Closed-Loop current control," *IEEE Trans. Ind. Appl.*, vol. 52, no. 4, pp. 3146–3158, Jul. 2016.

[9] H. K. Bae and R. Krishnan, "A study of current controllers and development of a novel current controller for high performance SRM drives," in *IAS '96. Conference Record of the 1996 IEEE Industry Applications Conference Thirty-First IAS Annual Meeting*, vol. 1, Oct. 1996, pp. 68–75 vol.1.